Spatio-temporal variations in High-Salinity Shelf Water production in Terra Nova Bay polynya, Antarctica

Seung-Tae Yoon[1], Won Sang Lee[1], Craig Stevens[2,3], Stefan Jendersie[4], SungHyun Nam[5], Sukyoung Yun[1], Chung Yeon Hwang[1], Gwang Il Jang[1], and Jiyeon Lee[1]

5   [1]Korea Polar Research Institute, Yeonsu-gu, Incheon 21990, Republic of Korea
[2]National Institute of Water and Atmospheric Research, Greta Point, Wellington 6021, New Zealand
[3]Department of Physics, University of Auckland, Auckland 1142, New Zealand
[4]Victoria University of Wellington, Wellington 6140, New Zealand
[5]Seoul National University, Gwanak-gu, Seoul 08826, Republic of Korea

10 *Correspondence to*: Seung-Tae Yoon (styoon@kopri.re.kr)

Abstract.

The formation of High-Salinity Shelf Water (HSSW), which is the major source of Antarctic bottom water (AABW), has been observed in Terra Nova Bay (TNB) in Antarctica. We believe a description of the spatio-temporal variation of salinity in TNB would help understand the production of HSSW in the region. Hence, the aim of this study is to investigate salinity variations
15 in the Drygalski Basin (DB) and eastern TNB close to Crary Bank of the Ross Sea. For this, we use the moored and profiled hydrographic data, as well as available wind and sea-ice products. We found that deep-ocean salinity in the eastern TNB (~660 m) and DB (~1,200 m) increases each year starting in September, and large amounts of salinity increase (> 0.04) were observed in 2016 and 2017. According to the velocity data observed at the same depths, the increases in salinity from September were due to the advection of HSSW from the coastal region of the Nansen ice shelf (NIS). The significant increases in salinity are
20 related to the formation of active HSSW, evidence of which can be found from the HSSW properties obtained in February 2017 and March 2018. In addition, we show that HSSW can locally formed in the upper layer (< 300 m) of the eastern TNB by wind-driven mixing. HSSW in the upper layer was only detected in 2016 and 2017 when much saltier HSSW was observed below 800 m. This indicates that brine supply related to the development of polynya by winds has contributed to the HSSW formation not only near the NIS, but also in the eastern TNB. Moreover, as compared with historical observations, salinity of
25 HSSW has been increasing since 2016 and, in 2018, it became similar with that in the early 2000. The observation of fluctuations such as this, which contrasts with past freshening, could contribute to estimating properties of recently formed AABW and improving the accuracy of both regional and global climate models.

1 Introduction

The strength of the global meridional overturning circulation is closely associated with the production of Antarctic bottom
30 water (AABW) (Jacobs, 2004; Johnson, 2008; Orsi et al., 1999, 2001), and approximately 25% of the AABW is produced in the Ross Sea (Orsi et al., 2002). In the western Ross Sea, as a result of the strong tidal movement of the Antarctic Slope Front across the shelf break and eddy interaction with the slope bathymetry, the circumpolar deep water (CDW) intrudes the

continental shelf to balance the High-Salinity Shelf Water (HSSW) off the ice shelf flow (Dinniman 2003; Budillon et al., 2011; St-Laurent et al., 2013; Stewart and Thompson, 2015; Jendersie et al., 2018). Model results suggest that the modified

35 CDW (MCDW) is advected as far south as Crary Bank, east of Terra Nova Bay (TNB) (Dinniman 2003, Jendersie 2018), although this has not been confirmed by observation. AABW is formed by the mixing of HSSW and CDW or MCDW (Budillon and Spezie, 2000; Budillon et al., 2011; Cincinelli et al., 2008; Gordon et al., 2009); therefore, HSSW is the major and densest parent water mass of AABW (Budillon and Spezie, 2000; Gordon et al., 2009).

Of the HSSW in the Ross Sea, 33% is produced in Terra Nova Bay polynya (TNBP) (Fusco et al., 2009; Rusciano et al., 2013;

40 Jendersie et al., 2018). TNBP (Fig. 1) is a coastal latent-heat polynya, on the surface of which dense water is formed (Fusco et al., 2002). The Drygalski ice tongue (DIT), which forms the southern boundary of TNBP, blocks the sea-ice moving from the south (Stevens et al., 2017). Katabatic winds blowing from the Nansen ice shelf (NIS) take the heat from the polynya, producing sea-ice in TNBP (Fusco et al., 2009; Tamura et al., 2016; Toggweiler and Samuels, 1995), which is responsible for the production of 3–4% of the total sea-ice in the Antarctic coastal polynyas (Tamura et al., 2016). The release of salty brine

45 as a result of sea-ice growth initiates the formation of HSSW and determines its properties (Fusco et al., 2009; Rusciano et al., 2013).

HSSW is mainly produced during the austral winter (April–October) when TNBP is most efficiently producing sea-ice in response to the persistent katabatic winds (Van woert, 1999; Rusciano et al., 2013; Sansiviero et al., 2017; Aulicino et al., 2018). TNBP does open in the austral summer, but HSSW is rarely formed in this period because of the cessation of sea-ice

50 production in the upper layer, along with ice-melting processes (Rusciano et al., 2013). According to the historical observations and the results of numerical modelling, the densest HSSW is formed from August to October and the maximum salinity of HSSW increases to approximately 34.86 (Buffoni et al., 2002; Fusco et al., 2009; Mathiot et al., 2012; Rusciano et al., 2013). Open ocean convection, which is led by wind-driven mixing, is suggested as the formation mechanism of HSSW (Buffoni et al., 2002; Mathiot et al., 2012). Besides the polynya activity, CDW transport in the Ross Sea continental shelf and water masses

55 flowing from the southern part of the DIT have been suggested as factors influencing the change in HSSW properties (Fusco et al., 2009; Stevens et al., 2017).

The coastal region of the NIS is considered as the primary location of HSSW formation in TNB, because this region is relatively shallow and katabatic winds blowing from across the NIS first meet the ocean surface. For this reason, salinity variations were investigated in the western part of the Drygalski Basin (DB) rather than the eastern TNB (Fusco et al., 2009; Rusciano et al.,

60 2013; Fig. 1). However, the shape of TNBP has varied over time, as shown from MODIS (Moderate-resolution Imaging Spectroradiometer) ice surface temperature imagery (Ciappa et al., 2012; Aulicino et al., 2018), indicating that the polynya activity could have spatial and temporal variations. Moreover, as suggested by model results, water masses in the deepest parts of the DB and eastern TNB could interact with those in the western Ross Sea via cyclonic circulation over Crary Bank (Jendersie et al., 2018; Fig. 1). In other words, HSSW accumulates in the deepest parts of DB and eastern TNB before being

65 transported predominantly north towards the shelf break. As a result, the formation of HSSW in the region could be spatially and temporally modulated by the influences of bathymetry, sea ice formation, and winds.

The present study uses ship-based *in situ* data collected in the austral summer (December–March) and hydrographic mooring data observed in the DB and eastern TNB during December 2014–March 2018, to explore the sub-polynya scale (~10s km) dynamics. In particular, we seek to answer the following research questions: (1) Does the nature of circulation in TNB influence

70   HSSW production? (2) Are there significant differences between salinity of the western (nearshore) and eastern (offshore) parts of TNB? and (3) Does wind variability play a role in salinity variation? We use the answers to these questions to pose a sequence of typical mechanistic scales for the polynya.

2 Data and Methods

2.1 Hydrographic measurements

75   We examined the spatio-temporal variation in the production of HSSW by using the time-series data from mooring stations in the eastern TNB (DITN) and the deepest depth of the DB (DITD) (blue diamond and magenta star in Fig. 1). The DITN mooring, which supports measurement of temperature, salinity, pressure, and ocean currents at three depths, using SBE37SM (Sea-Bird Scientific, Bellevue, WA, USA), RCM9 (Xylem, Inc., Rye Brook, NY, USA), and Aquadopp (Nortek, Norway) current meters (Fig. 2 and Table 1), has been continuously maintained since December 2014 (Table 1). Data from these devices

80   have been retrieved, downloaded, and maintained, and the instruments redeployed annually since. The redeployments are well collocated, so that the depths of the sensors' location in each observation period are almost the same during the three years (Fig. 2 and Table 1). During the second leg of DITN, the pressure value from an SBE37SM installed in a deep layer was recorded incorrectly; therefore, a nominal sensor depth of 660 m was used to calculate salinity. In addition, the DITD mooring was deployed for a single year during February 2017–March 2018, recording the same variables as DITN, but operating below

85   1,200 m (Fig. 2 and Table 1).

The temperature and salinity values obtained from these moorings were validated and corrected with conductivity–temperature–depth (CTD) casts in the moorings' position before the recovery and after the deployment of the DITN and DITD. The magnetic declination is corrected in the current direction and the velocities are low-pass filtered by monthly averaging. Current data observed with the RCM9 instrument during DITN mooring were used for consistency of data analysis, except the

90   uppermost current data of the third leg of DITN. Current data from RCM9 instrument at depth of 75 m were recorded till August 1, 2017; thereafter, Aquadopp current meter was used instead. Mean differences of the current direction (speed) between data observed from RCM9 and Aquadopp current meter at each depth are 2°, 3°, and 8° (1.8, 0.2, and –1.2 cm/s) during the third leg of DITN.

Full-depth CTD profile data measured by the icebreaking research vessel IBRV ARAON (Korea Polar Research Institute

95   (KOPRI)) during hydrographic surveys conducted were used to analyse the water mass properties of TNB. The profiles were recorded using an SBE 911 (Sea-Bird Electronics) along with CTD with dual temperature and conductivity sensors, and the sensors' calibration dates are within seven months of the observation dates. They were processed using standard methods recommended by SBE (Sea-Bird Electronics, Inc., 2014). Surveys on TNB were conducted during December 2014, December

2015, January–February 2017, and March 2018 (Table 1), although the locations of the profiles varied from year to year
depending on sea ice and priorities in cruise (Fig. 1). Profiles of horizontal currents (5-m interval) were measured using a
lowered acoustic Doppler current profiler (LADCP) instrument attached to the CTD frame. The LADCP data were processed
(Thurnherr, 2004) and velocities were de-tided using all ten available tidal components from CATS2008 (Circum-Antarctica
Tidal Simulation model) (Padman et al., 2002).

In order to directly compare the present work with results of previous studies (Budillon and Spezie, 2000; Budillon et al., 2002;
Budillon et al., 2011; Orsi and Wiederwohl, 2009), we use the practical salinity scale, rather than the thermodynamic equation
of seawater (TEOS)-10 (McDougall and Barker, 2017) results. We return to this point in Sect. 4. Potential densities (σ_θ) over
28 kg/m^3 were used as a criterion for the properties of the HSSW, to distinguish the HSSW from TNB ice shelf water (TISW)
(Fig. 3). TISW is the product of mixing between meltwater from ice-shelf melting and HSSW (Rusciano et al., 2013).

2.2 Wind and sea-ice data

The hourly wind data (2014–2018) observed at the Automatic Weather System (AWS) Manuela station (Ciappa et al., 2012;
Fig. 4a) were used to investigate the katabatic winds blowing over TNB. The AWS Manuela station is managed by the
Automatic Weather Station Program of the AMRC (Antarctic Meteorological Research Center) at the University of Wisconsin-
Madison. A katabatic wind event is defined as having a westerly wind direction of 225–315° and a wind speed of over 25 m/s.
The AWS Manuela station is situated such that it is within the pathway of the katabatic winds along the Reeves Glacier, making
it the best option to detect the katabatic winds blowing over TNB (Ciappa et al., 2012; Sansiviero et al., 2017).

The three-hourly 10-m wind and 2-m air-temperature data, provided by the ERA-Interim reanalysis data set (Dee et al., 2011),
are also used to identify the atmospheric conditions at TNB from January 2014 to March 2018. A grid size of 0.75° × 0.75°
is attributed to the data set. The averaged wind at the AWS Manuela station is approximately four times faster than that
provided by the ERA-Interim reanalysis data, but its direction is nearly the same with that at the grid located near Manuela
(about 6° difference) (Fig. 4a). ERA-Interim is a spatially smoothened product with a grid that is generally too coarse to
resolve steep glacier slopes, which may be the reason for the large difference in wind speed compared to the observed data
(Fusco et al., 2002; Dee et al., 2011). However, variations of eastward ($225° \leq \theta \leq 315°$) wind speed at Manuela are
significantly correlated (99% confidence level) with ERA-Interim retrieved values from TNB, including the region near DITN,
from July 2014 to March 2018 (correlation coefficient (r) > 0.70) (Fig. 4b). The eastward winds detected by the Manuela
station are synchronised with the wind in terms of occurrence and speed variability in all regions of TNB, despite the wind
speed being slower offshore. In addition, the daily air temperature observed in Manuela also has a significant r (> 0.90) with
that from ERA-Interim (Fig. 4b).

We also investigated the daily ARTIST (Arctic Radiation and Turbulence Interaction Study) sea-ice algorithm concentration
products with a grid spacing of 3.125 km from the Advanced Microwave Scanning Radiometer 2 data set (Spreen et al., 2008).
The selected data period is from July 2014 to March 2018, and the data domain is within the McMurdo Sound (Fig. 4a). We
applied the same continental masking obtained from the recent data and defined regions of sea-ice concentrations below 20%

as open water (Parkinson et al., 1999; Zwally et al., 2002). Lastly, the topographic data are from the International Bathymetric Chart of the Southern Ocean (IBSCO).

3 Results

135 ### 3.1 Deep-ocean salinity variations in TNB

Deep-ocean salinity observed in a mooring located in the eastern TNB (DITN, a blue diamond in Fig. 1) clearly exhibits interannual variations during 2015–2017 (Fig. 5a). Moreover, at approximately 660 m, during a span of three years, it significantly increases from 34.80 to 34.85, although there were some periods where the salinity decreased by 0.01–0.02 (Fig. 5a). The annual cycle of salinity begins increasing from September (Fig. 5a), and the change in salt contents (Fusco et al.,
140 2009) is estimated as 2.84, 7.64, and 5.23 µg salt/m^3/s from September to October of 2015, 2016, and 2017, respectively. Seawater properties during this period are included in the range of HSSW (blue dots in Fig. 6); therefore, the relatively large salt change in 2016 and 2017 is an indication of active HSSW formation during the austral winter in TNBP.

The evidence for active HSSW formation during April to October of 2016 and 2017 is still observed 3 and 5 months later, in January 2017 and March 2018, respectively (Fig. 3). The maximum salinity of HSSW found during January–February 2017
145 (2016/17) and in March 2018 (2017/18) was higher than that in the preceding surveys from April to October of 2016 and 2017, respectively (Fig. 3). The mean salinity of HSSW (σ_θ>28 kg/m^3) is calculated as 34.788 (σ=0.002), 34.785 (0.005), 34.801 (0.009), 34.815 (0.016) for each survey. Possible traces of MCDW are rare in the θ–S diagram (small panel in Fig. 3), so its effect on the changes of deep-ocean salinity in TNB are limited.

Vertical profiles of CTD also have features consistent with the θ–S diagram (Fig. 7). A quasi-homogeneous bottom layer
150 below 800 m represents the HSSW formed just before the austral winter (Fig. 7). Its salinity is relatively high in the 2016/17 and 2017/18 surveys (Fig. 7a; peak salinity, 34.83 and 34.85, respectively). Such a high-salinity water mass can form only in TNBP (Orsi and Wiederwohl, 2009). Thus, active HSSW formation in TNBP during the austral winters of 2016 and 2017 increases salinity of the water at 660 m of DITN mooring.

The latter two surveys were conducted in the late austral summer (January–February 2017 and March 2018); therefore, fewer
155 amounts of saline (dense) seawater in the upper depths and a strong salinity (density) gradient between the upper and lower layers were observed (Figs. 7a and 7c). The TISW, characterised by its potential temperatures lower than the freezing point at 50 m (approximately –1.95℃) and a salinity of approximately 34.73 (Budillon and Spezie, 2000), was observed from 300 to 600 m in 2016/17 and 2017/18, but not in the surveys in December (2014/15 and 2015/16) (Fig. 3 and Fig. 7b). It seems that the meltwater outflow from nearby ice shelves occurs in late summer.
160 However, the timing of salinity increase at the DITN occurs approximately 1–2 month later than that observed at mooring D (a triangle filled with black in Fig. 1) 33 km northwest of DITN (Rusciano et al., 2013). Saline seawater over 34.80 is only formed in TNBP, which is the reason behind the salinity increase measured in September. According to the current measurements obtained at the same depth (~660 m) as the salinity, flows are almost southward and slower than 4 cm/s (blue

arrows in Fig. 5b). Southwestward flows are mainly observed during the periods of increased salinity and southeastward flows
165   are episodically detected (Fig. 5b). The mean direction of the current is southwestward (191°) and its mean speed is
approximately 1.5 cm/s during the August–November period of three years (a blue arrow in Fig. 1). It is assumed that the
HSSW propagating into the eastern TNB for a month along the mean current, HSSW would come from 40 km of DITN in
northern direction. Moreover, HSSW is known to be formed near the NIS during the austral winter and propagates towards the
centre of TNB along 800–1,000-m isobaths (Fig. 1) (Rusciano et al., 2013). Thus, we conclude that the deep-ocean salinity in
170   the eastern TNB has increased since September due to the southward advection of HSSW from the centre of TNB (75°S, 165°E)
near mooring D.

The one-year of moored hydrographic data from the deepest depth of DB (DITD, a magenta star in Fig. 1) also captures the
salinity variation feature demonstrated during the third leg of DITN mooring (a magenta line in Fig. 5a). The salinity in the
deepest part of TNB also begins to increase from September, and the salt change from September to October 2017 is estimated
175   as 6.66 µg salt/m^3/s (Fig. 5a). Seawater properties observed from DITD are also included in the range of HSSW (magenta dots
in Fig. 6g–6i). However, northwestward currents are observed at a similar depth of salinity as that from DITD (1,222 m) during
the observation periods (Fig. 5b). The mean direction of the current is northwestward (300°), and its mean speed is
approximately 3.0 cm/s during August–November 2017 (a magenta arrow in Fig. 1). The maximum salinity measured at DITD
is larger than that at DITN (Fig. 5a), so the salinity increase in DITD is not related to the northwestward advection of HSSW
180   from the eastern TNB. Consequently, the current observed from DITD is considered as a part of the circulation in the deepest
parts of DB along the 1,000 m isobath. In other words, HSSW flowing into the DB from the NIS would circulate over the DB,
which is being detected at DITD since September 2017. The circulation in the DB is discussed further in Sect. 4.2.

3.2 Upper ocean salinity variations in the eastern TNB

Salinity was observed at around 75 and 273 m to investigate the variations in the upper water column of the eastern TNB (Fig.
185   8a). In contrast to the salinity at 660 m, salinity in the upper depths show a distinct seasonal variation. Salinity at both 75 m
and 273 m decreased, while salinity at the upper depth decreased to below 34.0 in February of each year (Fig. 8a). Thereafter,
the salinity of the two layers start mixing, as the salinity increases (decreases) at 75 (273) m. The salinity of the two layers
then increases in tandem from May to October (Fig. 8a). In December, mixing of the two layers ceases and their salinity
difference becomes larger again (Fig. 8a). The reduction in mixing is due to changes in buoyancy as a result of ice melting at
190   the surface during the austral summer.

We have noted that the period where these layers are well mixed has become shorter over time (Fig. 8a). If it is assumed that
the two layers are mixed when the σ_θ difference between the two layers is less than 0.1 kg/m^3 (~0.0005 kg/m^2) (Dong et al.,
2008), then early May in 2015, the end of April in 2016, and early April in 2017 are when the upper (at least to 273 m) water
column becomes isopycnal (Fig. 8b). From these times until October, salinities at the two depths become more highly
195   correlated than during the entire period. The salinity at 75 m has a 0.64, 0.58, and 0.62 correlation coefficient with that at 273
m during the 1st, 2nd, and 3rd legs (Table 1), respectively. However, for the periods in which salinity of two depths increase

together, r increases to 0.94, 0.88, and 0.93 (Fig. 8a), respectively. That is, salinity at two depths showed the most rapidly mixing during March-April 2017 among the three years and they are co-varied for the longest time until October, 2017. Moreover, the maximum salinity observed at 75 m and 273 m, during September–October also increased from 2015 to 2017

200   (34.774, 34.804, and 34.849), which is consistent with the trend of maximum salinity values observed in the deeper depths (Figs. 5a, 7 and 8a). HSSW is detected even in the upper depths during the August to October months in 2016 and 2017 (red and black dots in Figs. 6d–6i). On the contrary, the HSSW formation is rarely observed from August to October 2015, when the salinity increase is relatively small compared to that during the same period in 2016 and 2017 (Fig. 5a, red and black dots in 6a–6c).

205   The reasons for the greater increase in salinity in the upper depths could be considered as the formation of increasing amounts of dense water by brine rejection in the surface of the eastern TNB or by the advection of more saline water from other regions of TNB. According to current data obtained from the upper depths, westward currents are dominant at the two depths during December 2014–March 2018 (Fig. 8c), and the averaged speed (direction) of the currents from June to November is 7.4 cm/s (279°, westward) at 75 m, and 4.0 cm/s (270°, westward) at 273 m (Fig. 1). The currents could be the Ekman currents driven

210   by the northeastward winds blowing across the DIT (Fig. 4a) or the geostrophic currents induced by a latitudinal gradient of sea-surface height near the DIT. These would be the phenomena confined in coastal regions due to the existence of DIT (~300 m thickness). However, from these observations, only the upper water columns of the DITN seem to be affected by seawater from the eastern part of TNB during periods of increased upper level salinity. As identified in previous studies, farther away TNB, water masses are less saline due to mixing with CDW or due to MCDW intruding the western Ross Sea (Orsi and

215   Wiederwohl, 2009; Fusco et al., 2009; Budillon et al., 2011).

Thus, the salinity increase in the upper layers is related to the local brine supplied by sea-ice formation near the DITN region, rather than an advection of saline water from the western Ross Sea. As a result, the salinity (density) variations in the upper layers exhibit formation of dense water in the polynya via wind-driven mixing (Fig. 8a). In addition, the HSSW found in the upper layers during the months of August to October of 2016 and 2017 (Fig. 6d–6i, and 8a) implies that it could be formed by

220   the open-ocean convection in the eastern TNB, as suggested by model studies on TNBP (Buffoni et al., 2002; Mathiot et al., 2012).

3.3 Types of HSSW

We found that the deep-ocean salinity began to increase since September and the HSSW was detected in the upper depths of DITN during August–October (Fig. 5a and 6). From numerical modelling, a water column in TNB can be mixed to a depth of

225   750 m, forming an HSSW layer from the surface to this depth (Buffoni et al., 2002; Mathiot et al., 2012). That is, the increase of the deep-ocean salinity (660 m and 1,208 m) observed in 2016 and 2017 may be partly induced by the local formation of HSSW combined with the advected HSSW from the centre of TNB. However, the salinity time-series at 660 m is poorly correlated with the salinity variations in the upper depths of DITN during September–October 2016 and 2017 ($r < 0.30$), and its value is nearly as large as that observed in the upper water column (Figs. 6 and 8a). This means that the mixed layer does

230 not extend to 660 m in the eastern TNB and the higher salinity in the deep layer comes from the other regions in TNB, not the surface of DITN. Thus, in this case, HSSW formed in the eastern TNB needs to be distinguished from that produced in the coastal region of NIS. Its movement in the upper layers of TNB or its influence on the eastern TNB would be also interesting research topics; however, these types of HSSW are difficult to investigate with the current observational data used in this study.

3.4 Role of winds in TNBP

235 The wind in TNB is primarily westerly, and on an average creates an L-shaped polynya along the NIS and DIT, as shown by a contour line of 50% sea-ice concentration in Fig. 4a. The easterly winds measured at Manuela effectively open TNBP during the austral winters of the three years (Fig. 9). The r between daily wind speed (a blue line in Fig. 9) and the percentage of open water (sky blue bars in Fig. 9) is 0.46 during April to October of 2015, 2016, and 2017, which is significant at a 99% confidence level. In the austral winter of each year, the r is 0.49, 0.50, and 0.37, and all values are significant at a 99% confidence level

240 (Fig. 10). The period from the end of June to July 2017, when the open water did not expand greatly despite the strong winds, affects the estimation of the lowest r in the 2017 austral winter (Fig. 10c). The weak response of the polynya to these winds seems to be associated with a blocking effect of sea-ice in the offshore region (Tamura et al., 2016).

As inferred from the hydrographic surveys of TNB, HSSW had more actively formed in 2016 and 2017 than in 2014 and 2015; therefore, the deep-ocean salinity increased during late 2016 and 2017. It was suggested that the HSSW formation near the

245 mooring D is more dependent on the duration of single katabatic wind events, than on their frequency during April–October (Rusciano et al., 2013). In line with the wind observations by the Manuela station, among the three years, katabatic wind events occurred most frequently from April to October 2017 (210 events) (see wind speeds over 25 m/s in Fig. 10). The mean duration of a single katabatic wind event during these 7 months in the years 2015, 2016, and 2017 is estimated as 6.5, 7.0, and 7.7 hour, respectively. Moreover, the average length of time for which the polynya is open (> 20 % open water) during the same periods

250 is calculated as 5.8, 6.7, and 7.7 day, respectively. These data suggest that, during the four years of the study, the austral winter of 2017 is when the HSSW formation is the most active.

In addition, during September to October of 2016 and 2017, the upper layers of the eastern TNB also experienced the production of HSSW via convective processes after the development of a mixed layer. This means that the katabatic winds — considered pivotal to the development of a polynya (Fig. 9) and formation of HSSW near the NIS (Rusciano et al., 2013) —

255 generate wind-driven mixing in the eastern TNB and even produce HSSW. This could be partly explained by the relationship between the opening of TNBP by eastward winds and monthly change of salinity in the upper layers of DITN (positive values at 75 (273) m only shown as triangle (circle) black lines in Fig. 10). For example, the rate of salinity variation in April indicates a difference between mean salinities of water in April and March.

The rate of increase in salinity itself had increased during the April months of 2015 to 2017, due to stronger winds and a higher

260 percentage of open water in TNB (Fig. 10). The faster rate of change of salinity is led by faster mixing; therefore, in May 2017, the rate of change of salinity at both 75 and 273 m became positive (Fig. 8a and 10c). In May 2015 and 2016, the rate of change

of salinity is positive only at 75 m, while it was slightly larger in 2015 due to stronger winds (> 20 m/s) in early May (Figs. 10a and 10b).

Second, the high-speed winds (> 20 m/s) persistently blowing from late May to early July of 2016 create 50% more open sea
265 in TNBP, and the rate of change at the two depths becomes positive and larger in June 2016 (Fig. 10b). In June 2015, a positive rate is observed at the two depths, but only a slight increase at 273 m (~0.025/month) is observed due to relatively weak winds and polynya development compared to those in 2016 (Figs. 10a and 10b). In addition, salinity in the upper depths increased by over 40% in June 2017 in relation to the developments of TNBP, due to the winds blowing from early June to mid-June 2017 (Fig. 10c).

270 Third, both wind speed and open water area have decreased since June 2016. Consequently, the rate of change of salinity in the upper layers has remained below 0.05/month after June 2016 (Fig. 10b). On the contrary, the rate of increase in July 2015 and July 2017 became larger than in the previous month, because of higher wind speeds in July 2015 and July 2017 relative to June 2015 and June 2017 (Figs. 10a, 10c). However, after July 2015, the rate of increase has been constantly decreasing with the decrease of wind speed (Fig. 10a). During August–September 2017, the winds were still strong but could not effectively
275 open TNBP; therefore, the rate of change of salinity continued to decrease until October (Fig. 10c).

In summary, the mixing process during early 2017 is the fastest among the three years due to relatively strong winds from March to April, and the brine supply related to the polynya development with persistently strong winds during May–September 2017 would produce HSSW in the upper layers of the eastern TNB. The HSSW observed from September to October 2016 in the upper layers was fresher than that in 2017, which may be related to relatively weak winds and less brine supply in the late
280 2016. In 2015, HSSW is rarely found in the upper layers of DITN due to the absence of strong winds (> 25 m/s) during April–June 2015.

4 Discussions

Despite being a small, confined polynya, TNBP generates a substantial proportion of the global AABW. Understanding the supply of HSSW, and ultimately AABW, requires focus on processes at small scales from a regional perspective. Here,
285 behaviours of HSSW in TNB are investigated with the spatio-temporal variations in salinity observed in the eastern TNB and DB.

4.1 The present data in the context of previous analyse

The mooring D (Fig. 1) data of TNBP have shown seasonal variation of stratification in the water column and interannual variation of HSSW properties, which are closely associated with the polynya activity (Rusciano et al., 2013). This proves that
290 HSSW is produced during the austral winter, and a series of katabatic wind events in a certain period of time during the austral winter controls the HSSW properties. Data gathered for this study has revealed that HSSW could also form at the surface of the eastern TNB by wind-driven mixing and the same polynya process as that involved in the vigorous formation of HSSW

near the NIS. In addition, it was found that the large increases in salinity (> 0.04) observed in the deepest part of the DB and eastern TNB are due to the advection of HSSW and not the sinking HSSW directly from the surface at the mooring locations.

295   The HSSW formed near the NIS arrives at these depths within a few months; thus, HSSW is evenly distributed over TNB during the austral summer. In other words, the salinity of HSSW averaged in the eastern part of 164.5°E (34.802) shows no difference with that in the western part of 164.5°E (34.802) during the CTD observation periods. As a result, DITN, DITD, and four hydrographic surveys, along with the previous data from the mooring D, reveal spatio-temporal variations in the production of HSSW and the movement of HSSW in TNBP.

300   Hydrographic data have been collected from TNB for more than 20 years, and the longer-period variation of HSSW (~5 year) could be re-visited. However, each data set would contain an artificial uncertainty induced by the sensors' calibration date, sensor types, data processing tool, and other factors. Here, the potential temperature and practical salinity were used to ensure consistency of results with the previous studies; however, in future studies, HSSW in TNB need to be re-defined with a conservative temperature and absolute salinity (TEOS-10), to reduce uncertainties in the long-term trend of HSSW properties,

305   and find a quantitative relation with properties of water masses in the other regions.

4.2 Circulations in TNBP

For the austral summer (December–March), westward currents flowing along the DIT and northward currents along the NIS are found from the de-tided LADCP current data averaged over a depth range of 400–700 m (Fig. 11a). The currents resemble a cyclonic pattern together with the southeastward currents in the eastern TNB, despite southward currents heading for the

310   DIT along the 800–1000 m isobaths (Fig. 11a). However, southeastward currents crossing over from the NIS to the DIT were rarely observed in TNBP. The direction of the ocean current at 660 m of the DITN was stable during December 2014–March 2018 (Figs. 5b and 8c). Therefore, if the circulation pattern is assumed to be maintained throughout the year, then HSSW formed near the NIS may circulate clockwise, arriving in the DITN around September and inducing an increase in salinity, rather than directly propagating southeastward to the DITN. Furthermore, the wind-forcing-driven cyclonic gyre in the upper

315   layer of TNBP (Van woert et al., 2001) may induce an upwelling in the centre of TNB, which would hinder the development of horizontal flows in the central region of the gyre. The upwelling feature is visible in the vertical sections of four hydrographic surveys as upward-bending isopycnals in the upper layers (~400 m) of the mid-point of TNB (not shown).

The bottom currents in the DB flow under the influence of gravity (Jendersie et al., 2018), however, it is still not clear how the HSSW flowing under greater depths is circulated over the DB. Despite this, the LADCP data of December–March shows little

320   seasonal variation of the current direction at DITD, which can be an indication for the circulations in the DB region (> 1,000 m). The southwestward currents are shown in the northeastern part of the DB, while the northwestward and northeastward currents are identified in the southern and western region of the DB, according to the currents averaged from 900 m to the seafloor in the austral summer (Fig. 11b). The currents resemble a cyclonic circulation confined in the DB, which is different from the upper cyclonic gyre in TNB (van Woert et al., 2001). In other words, the HSSW propagating into the DB circulates

325   cyclonically in this region and can be detected at DITD from September. Together with the Ross Ice Shelf polynya, the DB

region is regarded as an outflow path of the HSSW towards the Ross Sea. Therefore, the circulation pattern in this region also needs to be investigated by acquiring more *in situ* ocean current data and ocean circulation models.

4.3 TNBP mechanical scales

It is useful to consider the range and scale of the physical processes active in TNBP. HSSW produced near the NIS spreads

330   horizontally into the eastern TNB (~35 km) and the DB (~25 km), at current speeds slower than 5 cm/s, in less than 2 months (from July to September). It also sinks vertically to the deepest depth of the DB (~1,200 m) at the same time. If it is assumed that the circulation in TNBP has a radius of 25 km (about one longitudinal degree), then it can be deduced that the HSSW circulates cyclonically about 80 km from the NIS to the eastern parts of TNB, which takes about one month at a current speed of 3 cm/s. In this case, the process of sinking would take less than one month at an average velocity of 0.05~0.07 cm/s. The

335   vertical velocity might be on a scale about 10^{-2} that of horizontal velocities in TNBP, which is regarded as a reasonable result in the ocean. TNBP usually forms as an L-shape, similar with model-derived polynya (Sansiviero et al., 2017; Fig. 4a); this means that the open water is mostly formed along the coasts near NIS (DIT) for approximately 75 (85) km. The average area for the polynya activity is approximately 1,600 km^2, by assuming the width of open water as 10 km from the coast through the 40% sea-ice concentration contour line (Fig. 4a). It accounts for about 5 % of the sea ice production area in Ross Ice Shelf

340   polynya (Cheng et al., 2017). In the eastern TNB, wind-driven mixing from the surface to a depth of 273 m occurs within 3 months (from March to May). The homogenous mixed layer is maintained above 273 m during the austral winter due to the persistent, strong winds, and the water column is stratified again from December. The opening of TNBP by westerly winds blowing from across the NIS occurs over the span of a day, and in this time the percentage of the open water can vary by up to $\pm 40\%$. The mean duration of the polynya opening is about 6.7 day during the austral winter in the analysis period. Salinity

345   values at 75 m and 273 m have increased from June or July (i.e., after the development of a mixed layer from the surface to a depth of 273 m), which indicates that brine rejection by sea-ice formation begins during that period.

4.4 Quantification of sea-ice production

The wind-driven polynya opening of TNBP is highly correlated with the monthly rate of change of salinity in the upper layers of the eastern TNB (Fig. 10). Therefore, the precise quantification of sea-ice production and brine formation in the polynya

350   region is needed for an in-depth understanding of dense-water formation processes. However, current data of brine supply by sea-ice formation in the polynya provided insufficient constraints. According to the previous results obtained using the ERA-Interim data set (Tamura et al., 2016), the estimated amounts of sea-ice production in TNBP has a high correlation ($r = 0.96$) with thin ice area (< 0.2 m), but exhibit a poor correlation ($r < 0.3$) with the offshore winds from the NIS and air temperature in TNB (see Table 1 in Tamura et al., 2016). This implies that the reanalysis data set did not reflect the air-sea heat exchange

355   induced by winds blowing over TNBP or the differences in temperature between the ocean and the atmosphere in TNBP. HSSW production was estimated using the changes in the heat flux averaged over TNB (Fusco et al., 2009); however, in near future, spatio-temporal variabilities in surface heat flux should be also investigated to determine the spatial variations in the

functioning of the polynya in TNB over time. Therefore, *in situ* data should be collected continuously to validate reanalysis data sets and suggest spatial and temporal relationships among wind speed, heat flux, sea-ice production, and the brine effect

360   in TNBP. In addition, algorithms should be developed to accurately process satellite data or new satellite observations to extract data on small-scale ice formations such as frazil ice.

5 Conclusions

This study investigated the spatial patterns and temporal changes in HSSW formation in TNBP during the period December 2014–March 2018 using a large, collaboratively produced data set. We found that HSSW that formed near the NIS flows along

365   cyclonic pattern currents in the deeper depths of TNBP and influences the eastern TNB and the deepest depth of the DB since September (Fig. 12). Due to this, the timing of the salinity increase is about two months later in the eastern (offshore) parts of TNB than in the western (nearshore) parts. Moreover, we found that katabatic winds blowing from across the NIS drive both the formation of HSSW near the NIS, and general increases in salinity by mixing layers of water and the polynya activity in the upper depths of the eastern TNB (Fig. 12). These findings answer the three research questions proposed in Sect. 1, and

370   complement to the results of previous research on HSSW formation in TNBP.

Large-scale freshening of AABW sources (including HSSW) has been reported in the Ross Sea and TNB in the recent decades (Jacobs et al., 2002; Fusco et al., 2009; Jacobs and Giulivi, 2010). The intensification of Southern Hemisphere westerlies (in association with a more positive phase of the Southern Annular Mode) was proposed as a possible driver of the ice-sheet melting and the corresponding seawater freshening upstream of the Ross Sea, because they induce an upwelling of the warm

375   water in the Amundsen and Bellingshausen Seas (Jacobs and Giulivi, 2010). In addition, sea-ice production variability is expected to play a large role in the HSSW formation (Jacobs and Giulivi, 2010).

The averaged salinity in a 10-m layer at 900-m depth shows larger values (> 0.025) in the 2016/17 and 2017/18 surveys than those in 2014/15 and 2015/16 surveys (Table 1). In other words, the salinity of HSSW formed in TNBP becomes increases again, and its value corresponds to those observed in the early 2000 (Fusco et al., 2009), although not an absolute salinity. The

380   HSSW formed in TNB could flow off the shelf break along Victoria Land (Cincinelli et al., 2008; Jendersie et al., 2018), which also contributes to volumes or properties of AABW in the western Ross Sea. However, the response of overturning circulations in the Southern Ocean to regional anomalies in buoyancy forcing have not been investigated (Rintoul, 2018), which is yet another limitation. Nevertheless, we will have to focus on the recent changes in salinity in the western Ross Sea, including TNB, with atmospheric and sea-ice conditions, and other observational results during the 2010s. Additionally, we will also

385   have to keep monitoring ocean changes in TNBP.

Data Availability

The observational data used in this study are held at the Korea Polar Data Center (https://kpdc.kopri.re.kr) and metadata DOIs are https://dx.doi.org/doi:10.22663/KOPRI-KPDC-00001062.1, https://dx.doi.org/doi:10.22663/KOPRI-KPDC-00000601.1,

390   https://dx.doi.org/doi:10.22663/KOPRI-KPDC-00001063.1, and https://dx.doi.org/doi:10.22663/KOPRI-KPDC-00000895.1
for CTD data; https://dx.doi.org/doi:10.22663/KOPRI-KPDC-00000895.1, https://dx.doi.org/doi:10.22663/KOPRI-KPDC-00001061.1, https://dx.doi.org/doi:10.22663/KOPRI-KPDC-00001065.1, and https://dx.doi.org/doi:10.22663/KOPRI-KPDC-00000896.1 for LADCP data; https://dx.doi.org/doi:10.22663/KOPRI-KPDC-00001060.1, https://dx.doi.org/doi:10.22663/KOPRI-KPDC-00000749.1, and https://dx.doi.org/doi:10.22663/KOPRI-KPDC-00000898.1 for DITN data; and https://dx.doi.org/doi:10.22663/KOPRI-KPDC-00000906.1 for DITD data. The wind data at the AWS

395   Manuela station and sea ice concentration data used in this manuscript are obtained from http://amrc.ssec.wisc.edu/aws/api/form.html, and https://seaice.uni-bremen.de/data/amsr2/asi_daygrid_swath/s3125/. The daily ERA-Interim reanalysis dataset is downloaded from https://apps.ecmwf.int/datasets/data/interim-full-daily/levtype=sfc/.

Author contribution

WSL and CS conceived and designed the experiments. STY, WSL, CS, SY, CYH, GIJ, and JL collected the observational data
400   in TNBP, and STY and CS processed them. STY, WSL, CS, SJ, SN, and CYH analysed the results and provided crucial insights into data interpretations. STY prepared the manuscript with contributions from all co-authors.

Competing Interests

The authors declare no conflicts of interest.

Acknowledgements

405   This study was sponsored by a research grant from the Korean Ministry of Oceans and Fisheries (KIMST20190361; PM19020) and the New Zealand Antarctic Research Institute, NZ Ministry of Business, Innovation and Employment, New Zealand National Institute of Water and Atmospheric Research (NIWA) (NZARI1401). We thank Gary Wilson, Christopher J. Zappa, Pierre Dutrieux, Brett Grant, Fiona Elliott and Alex Forrest for their support of this work through data collection and analysis as well as earlier versions of the paper.

410   **References**

Aulicino, G., Sansiviero, M., Paul, S., Cesarano, C., Fusco, G., Wadhams, P. and Budillon, G.: A new approach for monitoring the Terra Nova Bay polynya through MODIS Ice Surface Temperature Imagery and its validation during 2010 and 2011 winter seasons, Remote Sens., 10, 366, https://doi.org/10.3390/rs10030366, 2018.

Budillon, G. and Spezie, G.: Thermohaline structure and variability in the Terra Nova Bay polynya, Ross Sea, Antarct. Sci.,
415   12(4), 493–508, http://doi.org/10.1017/S0954102000000572, 2000.

Budillon, G., Cordero, S. G. and Salusti, E.: On the dense water spreading off the Ross Sea Shelf (Southern Ocean), J. Mar. Syst., 35, 207–227, https://doi.org/10.1016/S0924-7963(02)00082-9, 2002.

Budillon, G., Castagno, P., Aliani, S., Spezie, G. and Padman, L.: Thermohaline variability and Antarctic bottom water formation at the Ross Sea shelf break, Deep-Sea Res. Part I, 58, 1002–1018, http://doi.org/10.1016/j.dsr.2011.07.002, 2011.

420 Buffoni, G., Cappelletti, A. and Picco, P.: An investigation of thermohaline circulation in the Terra Nova Bay polynya, Antarct. Sci., 14(1), 83–92, http://dx.doi.org/10.1017/S0954102002000615, 2002.

Cheng, Z., Pang, X., Zhao, X. and Tan, C.: Spatio-temporal variability and model parameter sensitivity analysis of ice production in Ross Ice Shelf polynya from 2003 to 2015, Remote Sens., 9, 934, 1–20, https://doi.org/10.3390/rs9090934, 2017.

Ciappa, A., Pietranera, L. and Budillon, G.: Observations of the Terra Nova Bay (Antarctica) polynya by MODIS ice surface

425 temperature imagery from 2005 to 2010, Remote Sens. Environ., 119, 158–172, http://doi.10.1016/j.rse.2011.12.017, 2012.

Cincinelli, A., Martellini, T., Bittoni, L., Russo, A., Gambaro, A. and Lepri, L.: Natural and anthropogenic hydrocarbons in the water column of the Ross Sea (Antarctica), J. Mar. Syst., 73, 208–220, https://doi.org/10.1016/j.jmarsys.2007.10.010, 2008.

Dee, D. P., Uppala, S. M., Simmons, A. J., Berrisford, P., Poli, P., Kobayashi, S., Andrae, U., Balmaseda, M. A., Balsamo, G., Bauer, P., Bechtold, P., Beljaars, A. C. M., Berg, L. V., Bidlot, J., Bormann, N., Delso, C., Dragani, R., Fuentes, M., Geer, A.

430 J., Haimberger, L., Healy, S. B., Hersbach, H., Holm, E. V., Isaksen, L., Kallberg, P., Kohler, M., Matricardi, M., McNally, A. P., Monge-Sanz, B. M., Morcrette, J. J., Park. B. K, Peubey, C., Rosnay, P., Tavolato, C., Thepaut, J. N. and Vitart, F.: The ERA-Interim reanalysis: configuration and performance of the data assimilation system, Q. J. R. Meteorol. Soc., 137, 553–597, https://doi.org/10.1002/qj.828, 2011.

Dinniman, M. S., Klinck, J. M. and Smith, W. O. Jr.: Cross-shelf exchange in a model of the Ross Sea circulation and

435 biogeochemistry, Deep-Sea Res. Part II, 50, 3103–3120, https://doi.10.1016/j.dsr2.2003.07.011, 2003.

Dong, S., Sprintall, J., Gille, S. T. and Talley, L.: Southern Ocean mixed-layer depth from Argo float profiles, J. Geophys. Res., 113, C06013, http://doi.org/10.1029/2006JC0gordon04051, 2008.

Fusco, G., Budillon, G. and Spezie, G.: Surface heat fluxes and thermohaline variability in the Ross Sea and in Terra Nova Bay polynya, Cont. Shelf Res., 29, 1887–1895, http://dx.doi.org/10.1016/j.csr.2009.07.006, 2009.

440 Fusco, G., Flocco, D., Budillon, G., Spezie, G. and Zambianchi, E.: Dynamics and variability of Terra Nova Bay polynya, Mar. Ecol., 23, 201–209, https://doi.org/10.1111/j.1439-0485.2002.tb00019.x, 2002.

Gordon, A. L., Orsi, A. H., Muench, R., Huber, B. A., Zambianchi, E. and Visbeck, M.: Western Ross Sea continental slope gravity currents, Deep-Sea Res. Part II, 56, 796–817, http://doi.org/10.1016/j.dsr2.2008.10.037, 2009.

Jacobs, S. S.: Bottom water production and its links with the thermohaline circulation, Antarct. Sci., 16, 427–437,

445 https://doi.org/10.1017/S095410200400224X, 2004.

Jacobs, S. S. and Giulivi, C. F.: Large Multidecadal salinity trends near the Pacific-Antarctic Continental margin, J. Clim., 23, 4508-4524, https://dx.doi.org/10.1175/2010JCLI3284.1, 2010.

Jacobs, S. S., Giulivi, C. F., and Mele, P. A.: Freshening of the Ross Sea during the late 20th century, Science, 297, 386-388, https://dx.doi.org/ 10.1126/science.1069574, 2002

450 Jendersie, S., Williams, M. J. M., Langhorne, P. J. and Robertson, R.: The density-driven winter intensification of the Ross Sea circulation, J. Geophys. Res. Oceans, 123, 1-23, https://doi.org/10.1029/2018JC013965, 2018.

Johnson, G. C.: Quantifying Antarctic Bottom Water and North Atlantic Deep Water volumes, J. Geophys. Res. Oceans, 113, C05027, https://doi.org/10.1029/2007JC004477, 2008.

Mathiot, P., Jourdain, N. C., Barnier, B., Gallee, H., Molines, J. M., Sommer, J. L. and Penduff, T.: Sensitivity of coastal polynyas and high-salinity shelf water production in the Ross Sea, Antarctica, to the atmospheric forcing, Ocean Dyn., 62, 701-723, http://dx.doi.org/10.1007/s10236-012-0531-y, 2012.

McDougall, T. J. and Barker, P. M.: Getting started with TEOS-10 and the Gibbs Seawater (GSW) Oceanographic Toolbox – version 3.06.3, 28pp., SCOR/IAPSO WG127, ISBN 978-0-646-55621-5, 2017.

Orsi, A. H., Jacobs, S. S., Gordon, A. L. and Visbeck, M.: Cooling and ventilating the Abyssal Ocean, Geophys. Res. Lett., 28(15), 2923–2926, https://doi.org/10.1029/2001GL012830, 2001.

Orsi, A. H., Johnson, G. C. and Bullister, J. L.: Circulation, mixing, and production of Antarctic Bottom Water, Prog. Oceanogr., 43, 55–109, https://doi.org/10.1016/S0079-6611(99)00004-X, 1999.

Orsi, A. H., Smethie Jr., W. M. and Bullister, J. L.: On the total input of Antarctic waters to the deep ocean: a preliminary estimate from chlorofluorocarbon measurements, J. Geophys. Res. Oceans, 107(C8), 3122, https://doi.org/10.1029/2001JC000976, 2002.

Orsi, A. H. and Wiederwohl, C. L.: A recount of Ross Sea waters, Deep-Sea Res. Part II, 56, 778–795, http://doi.org/10.1016/j.dsr2.2008.10.033, 2009.

Padman, L., Fricker, H. A., Coleman, R., Howard, S. and Erofeeva, L.: A new tide model for the Antarctic Ice shelves and Seas, Ann. Glaciol., 34, 1-14, https://doi.org.10.3189/172756402781817752, 2002.

Parkinson, C. L., Cavalieri, D. J., Gloersen, P., Zwally, H. J. and Comiso, J. C.: Arctic sea ice extents, areas, and trends, 1978–1996, J. Geophys. Res. Oceans, 104(C9), 20,837–20,856, https://doi.org/10.1029/1999JC900082, 1999.

Rintoul, S. R.: The global influence of localized dynamics in the Southern Ocean, Nature, 558, 209–218, http://doi.org/10.1038/s41586-018-0182-3, 2018.

Rusciano, E., Budillon, G., Fusco, G., and Spezie, G.: Evidence of atmosphere–sea ice–ocean coupling in the Terra Nova Bay polynya (Ross Sea–Antarctica), Cont. Shelf Res., 61–62, 112–124, http://dx.doi.org/10.1016/j.csr.2013.04.002, 2013.

Sansiviero, M., Maqueda, M. A. M., Fusco, G., Aulicino, G., Flocco, D. and Budillon, G.: Modelling sea ice formation in the Terra Nova Bay polynya, J. Mar. Syst., 166, 4–25, http://dx.doi.org/10.1016/j.jmarsys.2016.06.013, 2017.

Sea-Bird Electronics, Inc.: Seasoft V2: SBE data processing (User's Manual, pp. 1–174). Bellevue, Washington, USA, 2014.

Spreen, G., Kaleschke, L. and Heygster, G.: Sea ice remote sensing using AMSR-E 89 GHz channels, J. Geophys. Res. Oceans, 113, C02S03, http://doi.org/10.1029/2005JC003384, 2008.

Stevens, C., Lee, W. S., Fusco, G., Yun, S., Grant, B., Robinson, N. and Hwang, C. Y.: The influence of the Drygalski Ice Tongue on the local ocean, Ann. Glaciol., 58(74), 51–59, https://doi.org/10.1017/aog.2017.4, 2017.

Stewart, A. L. and Thompson, A. F.: Eddy-mediated transport of warm Circumpolar Deep Water across the Antarctic shelf break, Geophys. Res. Lett., 42, 432–440, https://doi.org/10.1002/2014GL062281, 2015.

485   St-Laurent, P. Klinck, J. M. and Dinniman, M. S.: On the role of coastal troughs in the circulation of warm Circumpolar Deep Water on Antarctic shelves, J. Phys. Oceanogr., 43(1), 51-64, https://doi.org/10.1175/JPO-D-11-0237.1, 2013.

Tamura, T., Ohshima, K. I., Fraser, A. D. and Williams, G. D.: Sea ice production variability in Antarctic coastal polynyas, J. Geophys. Res. Oceans, 121, 2967–2979, https://doi.org/10.1002/2015JC011537, 2016.

Toggweiler, J. R. and Samuels, B.: Effect of sea ice on the salinity of Antarctic bottom waters, J. of Phys. Oceanogr., 25,
490   1980–1997, https://doi.org/10.1175/1520-0485(1995)025<1980:EOSIOT>2.0.CO;2, 1995.

Thurnherr, A. M.: How to Process LADCP Data with the LDEO Software. New York: Columbia University. ftp://ftp.ldeo.columbia.edu/pub/LADCP/HOWTO/LDEO_IX.pdf, 2014.

Van Woert, M. L.: Wintertime dynamics of the Terra Nova Bay polynya, J. Geophys. Res. Oceans, 104, C4, 7753–7769, https://doi.org/10.1029/1999JC900003, 1999.

495   Van Woert, M. L., Meier, W. N., Zou, C.-Z., Archer, A., Pellegrini, A., Grigioni, P. and Bertola, C.: Satellite observations of upper-ocean currents in Terra Nova Bay, Antarctica. Ann. Glaciol., 22, 407–412, https://doi.org/10.3189/172756401781818879, 2001.

Zwally, H. J., Comiso, J. C., Parkinson, C. L., Cavalieri, D. J. and Gloersen, P.: Variability of Antarctic sea ice 1979–1998. J. Geophys. Res. Oceans, 107(C5), 3041, 9-1–9-19, https://doi.org/10.1029/2000JC0007, 2002.

500
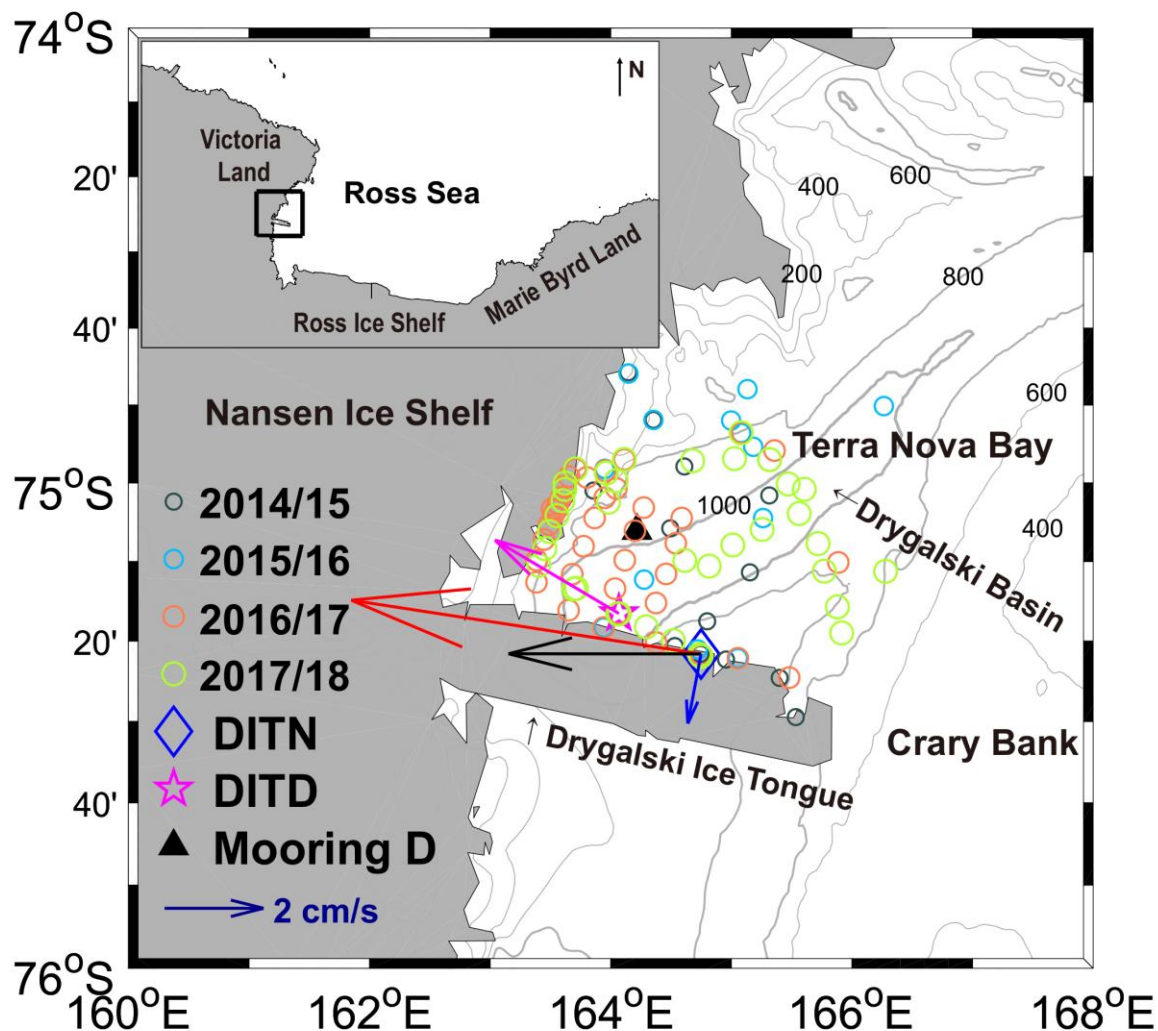
Figure 1: Topographic map of Terra Nova Bay (TNB). The location of TNB in the Ross Sea is shown in an upper-left panel. The bold grey line indicates 1000-m isobaths and the interval between the thinner grey lines is 200 m. Conductivity-temperature-depth (CTD) stations in the austral summers, 2014, 2015, 2017, and 2018 are denoted by open circles. The averaged current vector from August to November at 660 m of DITN (1222 m of DITD) is denoted by a blue (magenta) arrow. The red (black) arrow indicates the mean current vector from June to November at 75 (273 m) of DITN. The reference velocity (2 cm s^{-1}) is shown by the blue arrow in the left-bottom.
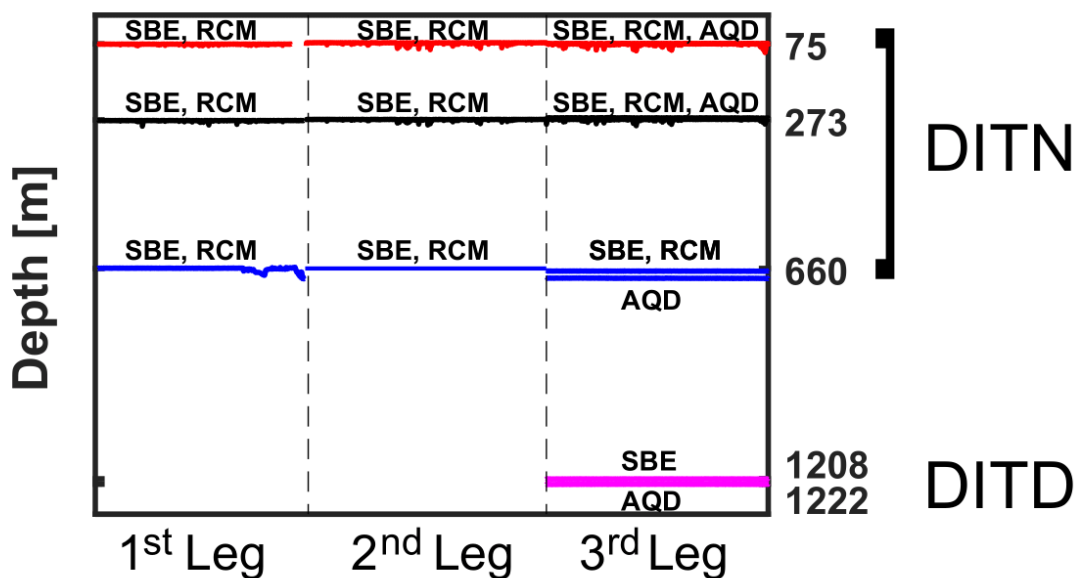
Figure 2: The recorded depth of sensors during the three observation legs. The red, black, and blue lines show the depth time series for sensors at the upper-, mid-, and deep-layer of DITN.

510 The recorded depth of sensors from DITD are also shown by a magenta line. The SBE, RCM, and AQD represent the SBE37SM, RCM9, and Aquadopp current meters, respectively (see details in Table 1).
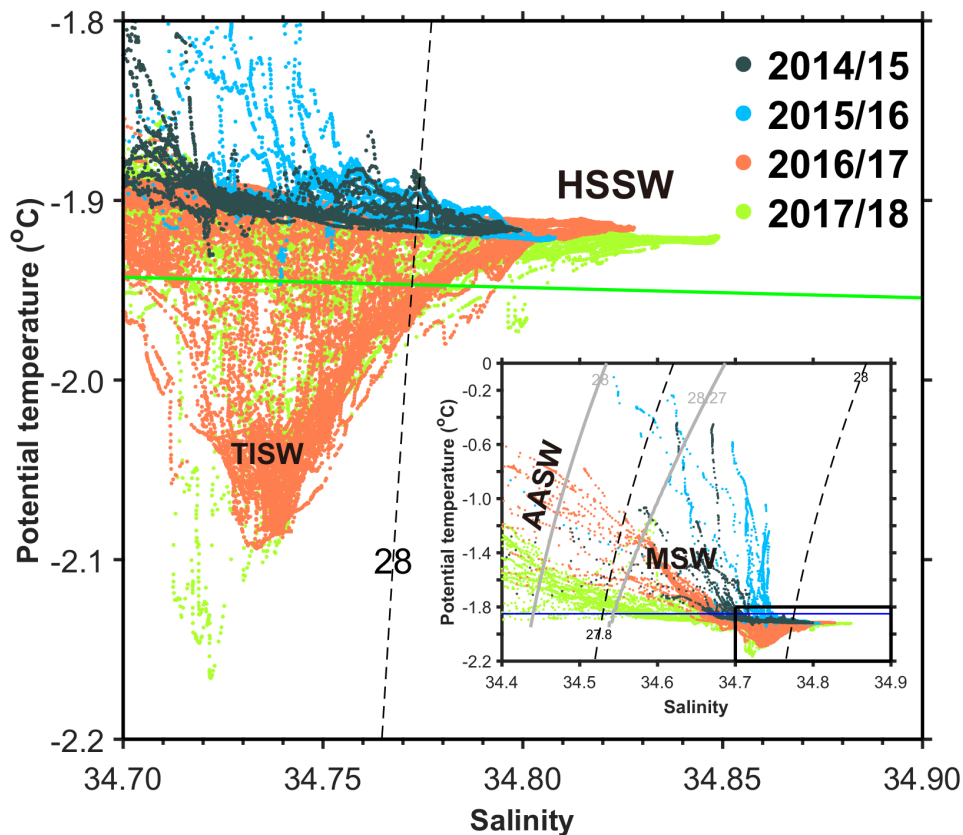
Figure 3: A zoomed-in plot of the θ-S (potential temperature–salinity) diagram for CTD data observed in TNB during each observation period. The green solid line denotes the freezing point at 50 m depending on salinity, and the black dashed line indicates an isopycnal. The full range θ-S diagram is shown in the small lower-right panel. The black box and blue line indicate the ranges of the magnified plot, and the –1.85 °C isotherm, respectively. The grey solid lines denote 28 and 28.27 kg m^{-3} neutral density (γ^n) surfaces. AASW, MSW, TISW, and HSSW represent the Antarctic Surface Water, Modified Shelf Water, Terra Nova Bay Ice Shelf Water, and High-Salinity Shelf Water, respectively.
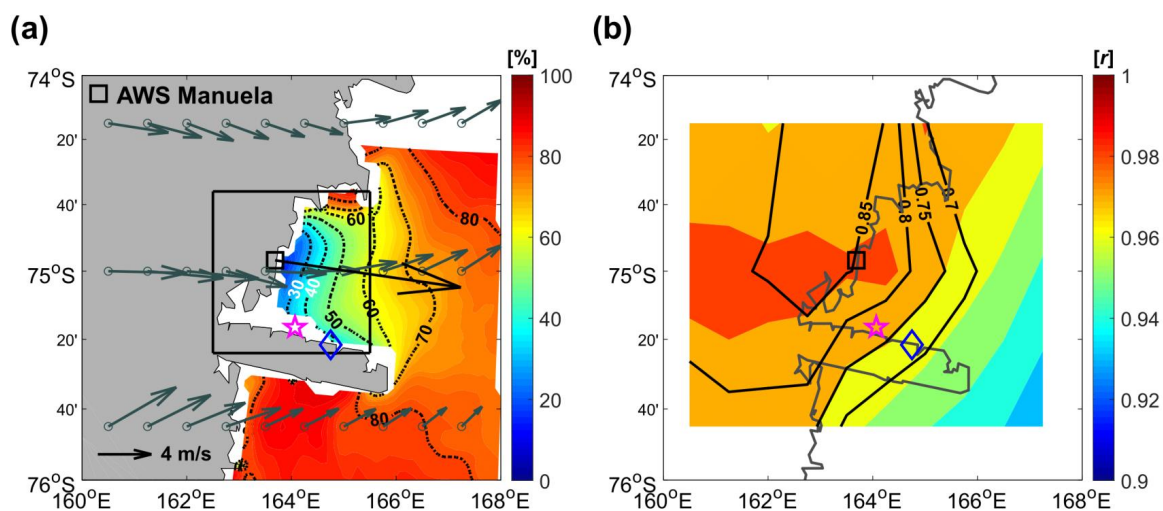
520 **Figure 4:** (a) Spatial distributions of averaged sea-ice concentrations from July 2014 to March 2018. The interval of dotted contour lines is the 10% concentration. The black square (blue diamond and magenta star) indicates the Automatic Weather System (AWS) Manuela station (DITN and DITD). The dark-grey (black) arrow is a mean wind vector during July 2014– March 2018 by using ERA-Interim data (data from AWS Manuela station). A black box denotes an averaged region for sea ice concentrations. (b) Spatial distributions of correlation coefficients (r) between daily air temperature from ERA-Interim and Manuela during July 2014–March 2018. The black solid contour lines indicate the horizontal distributions of r between daily eastward wind speed from ERA-Interim and Manuela during the same period.
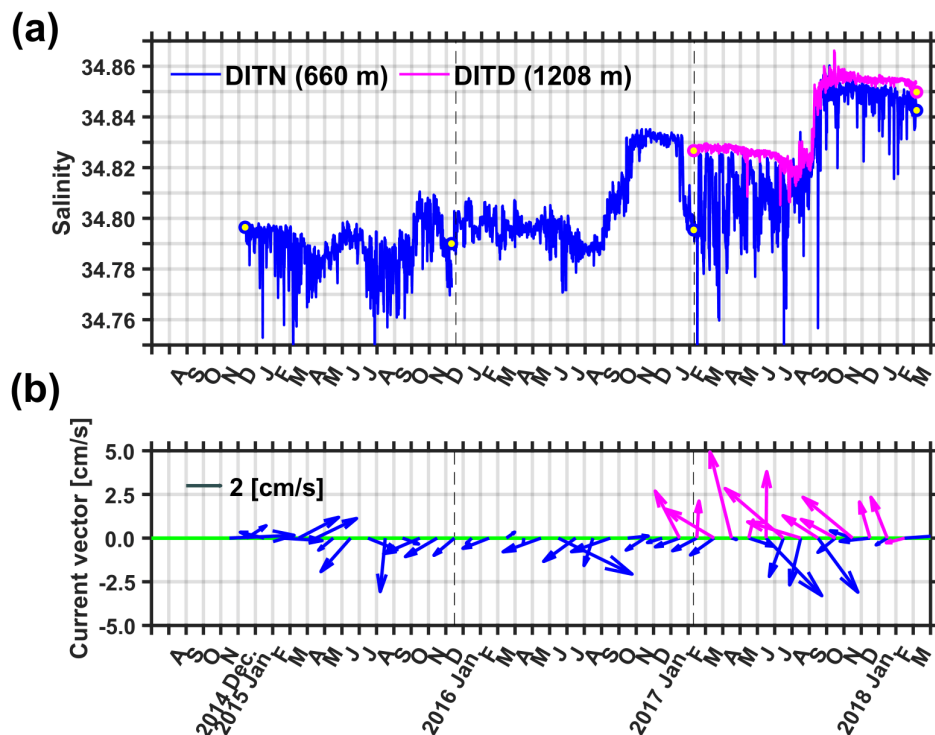
525

Figure 5: (a) Time series of deep-ocean salinity observed in DITN (blue) and DITD (magenta) from December 2014 to March 2018. The blue (magenta) circles filled with yellow indicate the averaged salinity in a 5-m layer at the bottom obtained using CTD data observed near DITN (DITD). The black dashed line divides periods of each lag of the moorings (see details in Table. 1). (b) Monthly mean current vectors at 660 m of DITN and 1222 m of DITD are indicated by blue and magenta arrows.
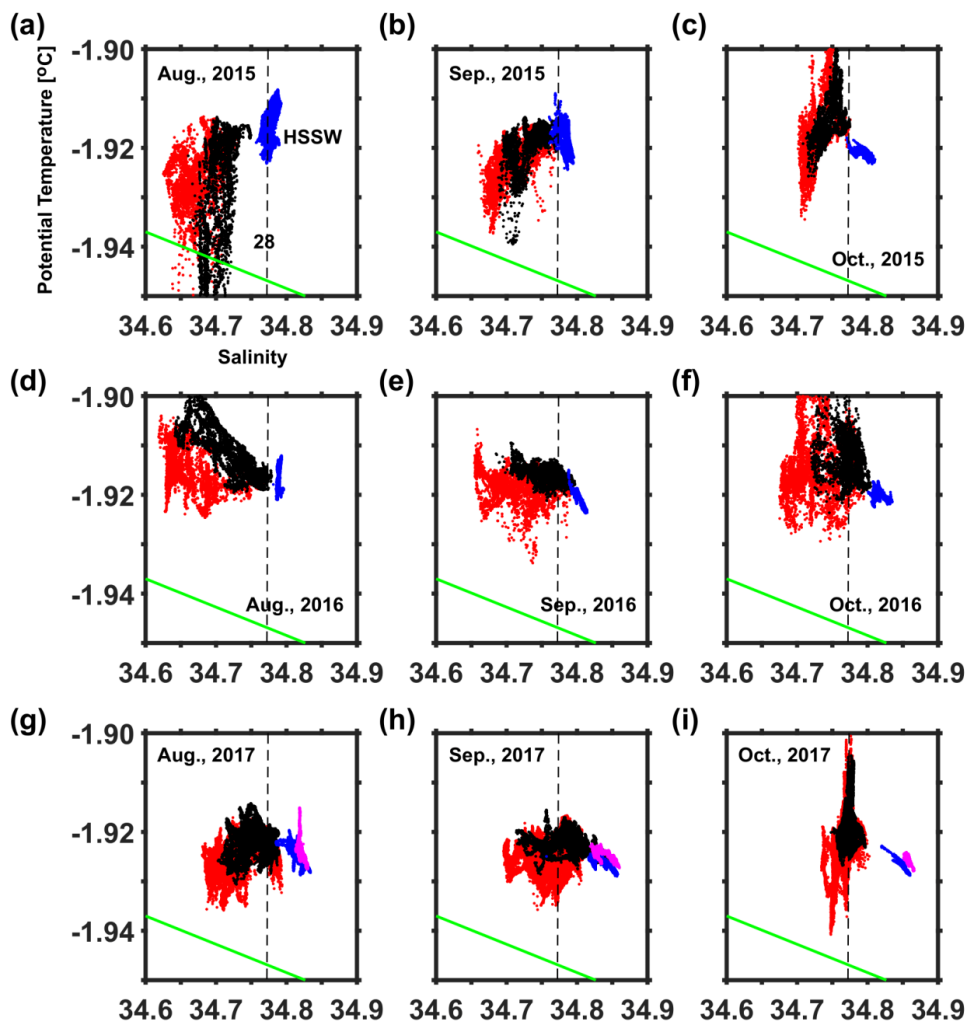
530

Figure 6: (a) A magnified version of the θ-S (potential temperature–salinity) diagram for data from DITN and DITD in August 2015. Red, black, and blue dots are θ-S at 75, 273, and 660 m. The green thin line denotes the freezing point at 50 m depending on salinity, and the black dashed line indicates $\sigma_\theta = 28.00\,\mathrm{kg\,m^{-3}}$. (b) The same as Fig. 6a, but for September 2015. (c) The same as Fig. 6a, but for October 2015. (d-f) The same as Fig. 6a-6c, but for August-October 2016. (g-i) The same as Fig. 6a-6c, but for August-October 2017. Magenta dots are θ-S at 1208 m.
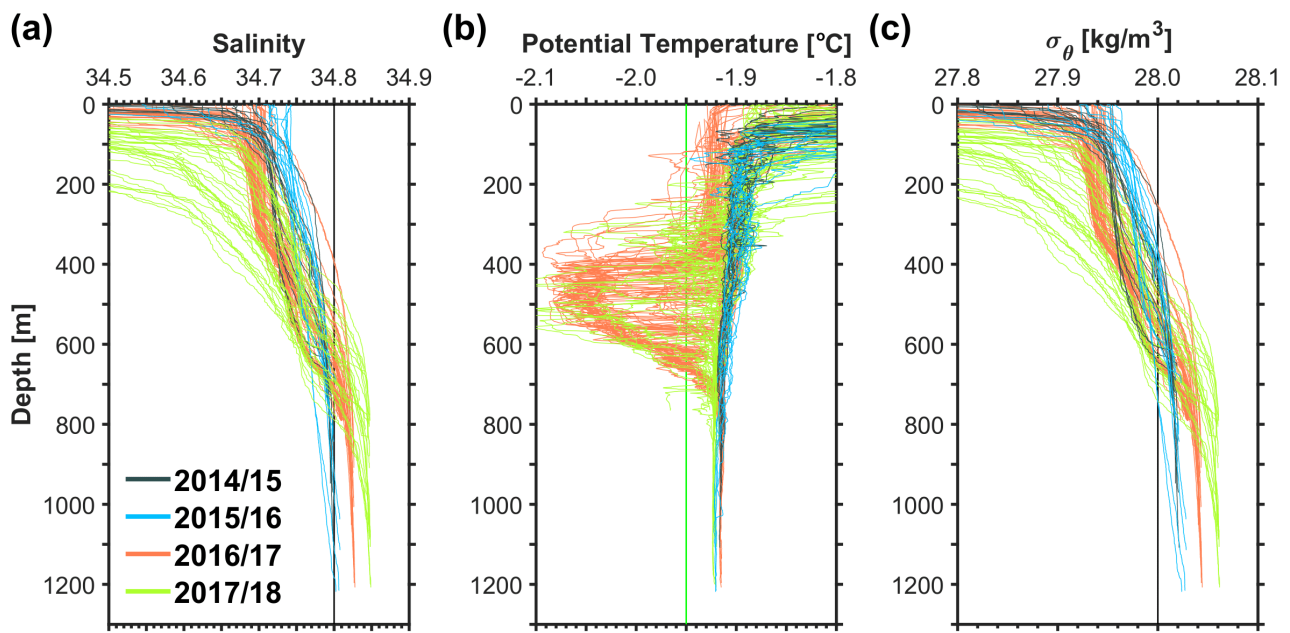
Figure 7: (a) Vertical salinity profiles at each observation period. The black solid line indicates 34.8 (b) The same as Fig. 7a, but for potential temperature, and the green solid line denotes $-1.95\,°C$. (c) The same as Fig. 7a, but for potential density (σ_θ), and the black solid line means $28.0\,kg\,m^{-3}$
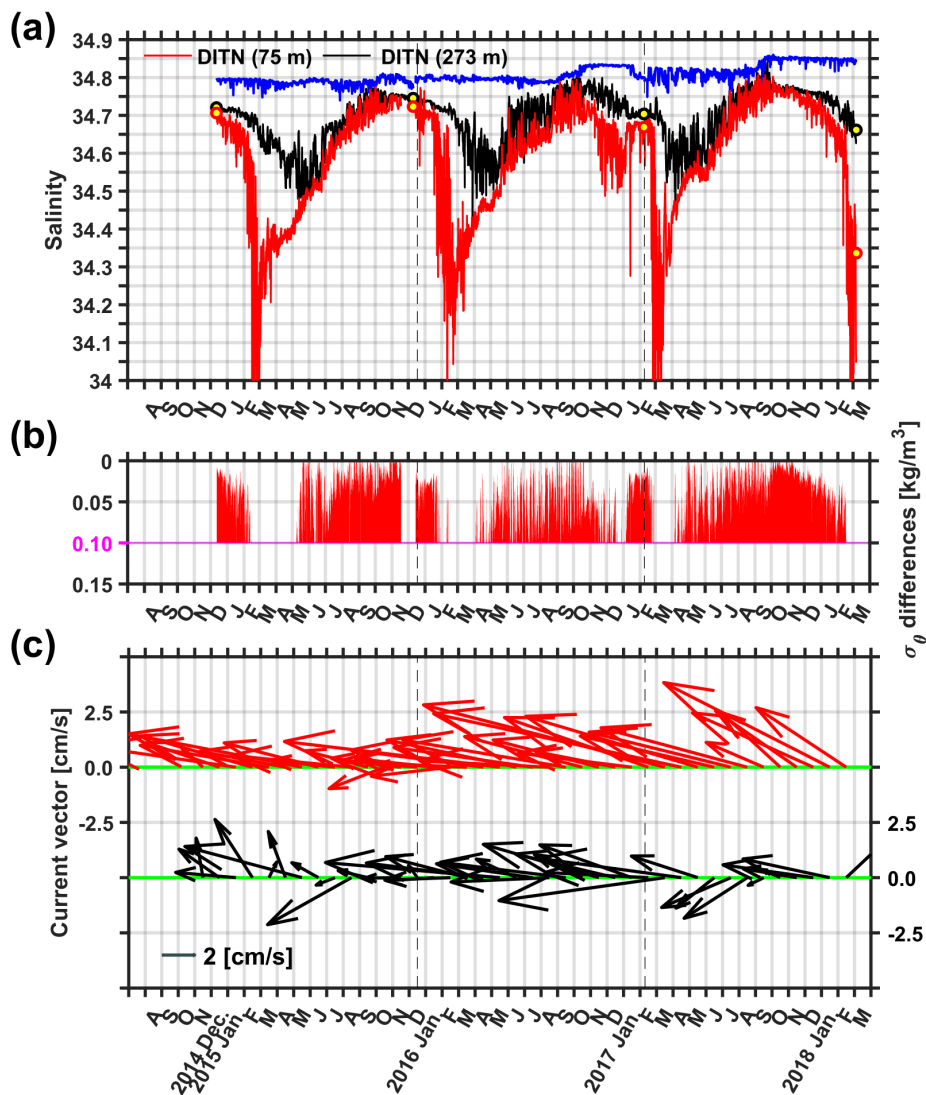
Figure 8: (a) Salinity time-series at three depths from DITN. The red (black) circles filled with yellow are averaged salinity in a 5-m layer at 75 (273) m obtained using CTD data observed near DITN. The black dashed line divides periods of each lag of moorings (see details in Table. 1). (b) Potential density (σ_θ) differences lower than 0.10 kg m^{-3} between σ_θ at 75 and 273 m. A magenta line indicates 0.10 kg m^{-3} difference. (c) Monthly mean current vectors at 75 and 273 m of DITN are indicated by red and black arrows.
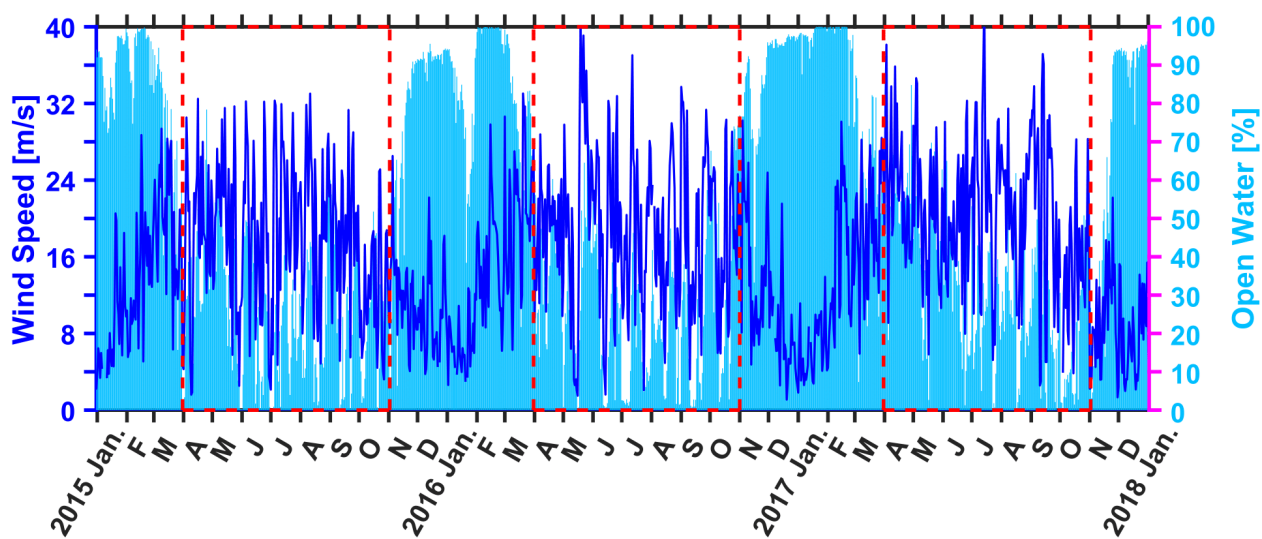
545

Figure 9: Time-series from 2015 to 2017 for daily eastward (225° < θ < 315°) wind speed from Manuela (blue line), and the daily percentage of open water averaged in a black box in Fig. 4a (sky blue bar). Red dashed boxes indicate a time domain of Fig. 10a, 10b, and 10c.
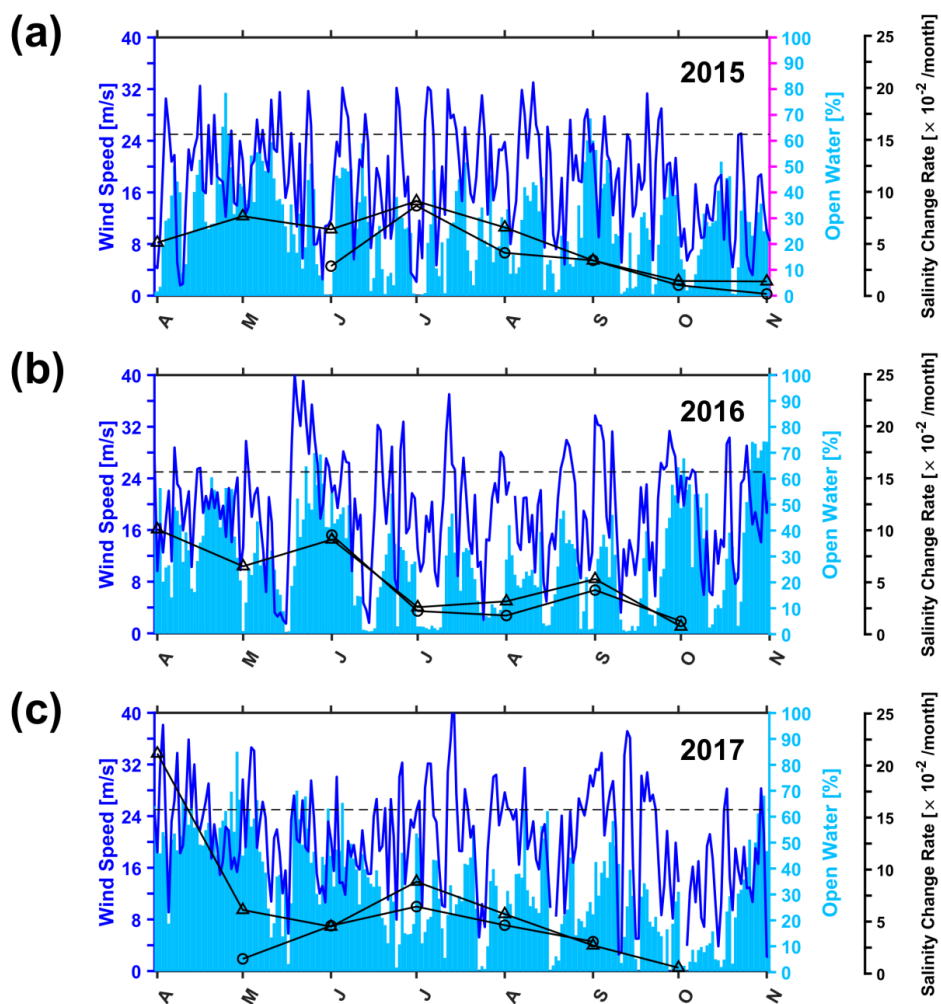
Figure 10: (a) The same as Fig. 9, but for the 2015 austral winter. The black triangle (circle) line indicates positive monthly
550   salinity changes at 75 (273) m obtained by the salinity difference between two months. The black dashed line indicates 25 m
s⁻¹ wind speed. (b) The same as Fig. 10a, but for 2016. (c) The same as Fig. 10a, but for 2017.
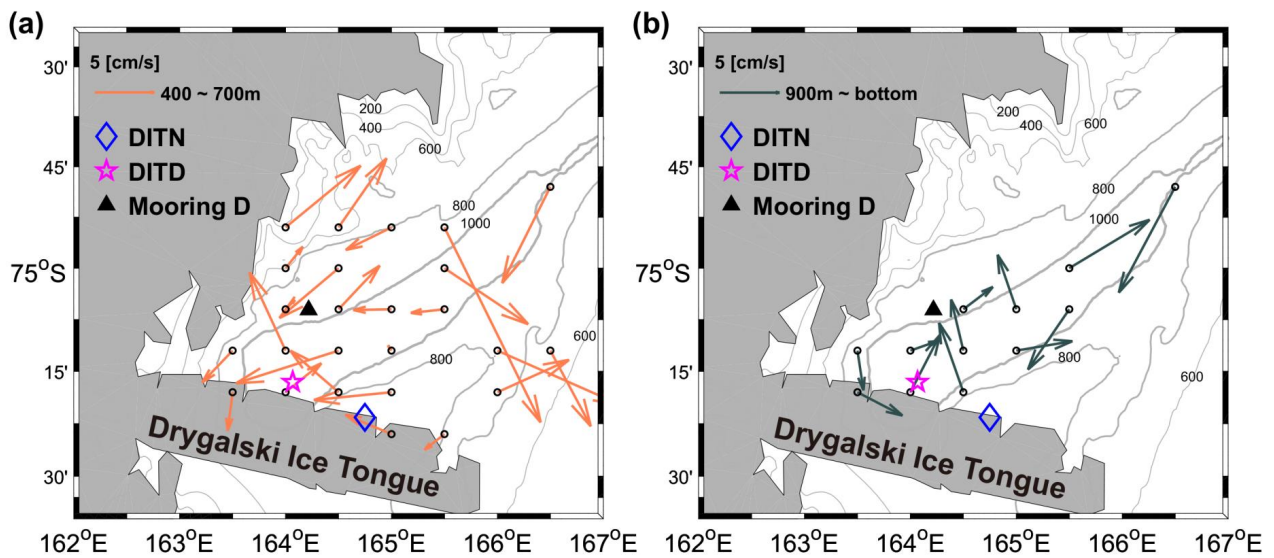
Figure 11: (a) Mean currents in a range of 400–700 m during four hydrographic surveys (see details in Table 1). The LADCP data are arranged by averaging on a 0.5° × 0.1° grid. (b) The same as Fig. 11a, but for in a range of 900 m–bottom.
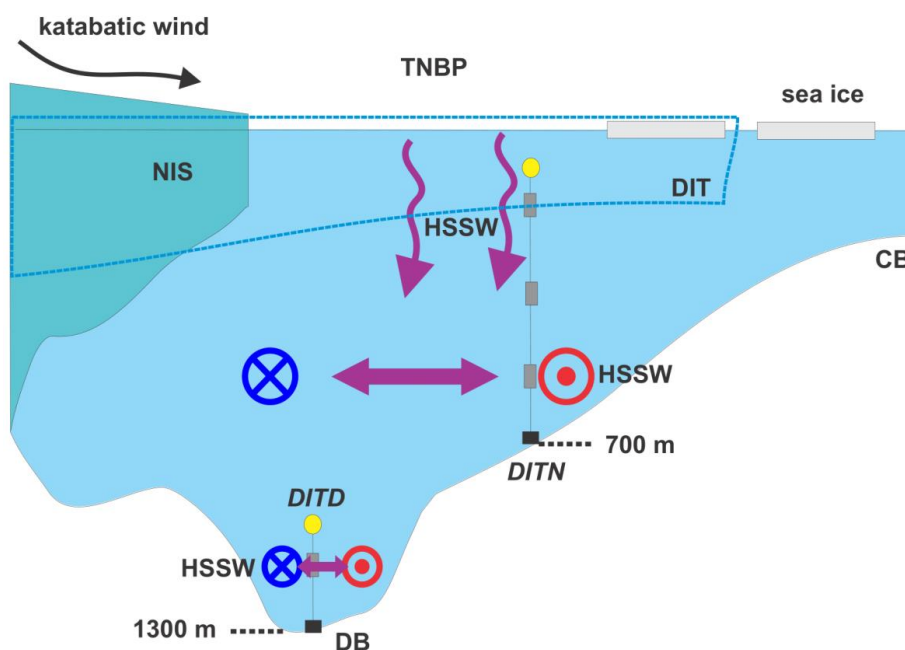
555

Figure 12: A schematic of the spatio-temporal variations in the production of HSSW in TNBP. The downward arrows show HSSW formation from the surface through wind-driven mixing and polynya operation. The horizontal bi-directional arrows indicate that the HSSW that formed near the Nansen Ice Shelf (NIS) advects the deepest depth of the eastern Terra Nova Bay (DITN) and the deepest depth of the Drygalski Basin (DITD) via cyclonic pattern flows in TNBP. The blue (red) circle

560   represents incoming (outgoing) flow. DB, CB and DIT indicate the Drygalski Basin, Crary Bank and Drygalski Ice Tongue, respectively.

Table 1. Information for four oceanographic surveys and data observed from DITN and DITD. U, V, T, C, and P represent the east-west current speed, north-south current speed, temperature, conductivity, and pressure, respectively. S, R, and A are instrument's abbreviations for SBE37SM, RCM9, and Aquadopp current meter, respectively.

565

Survey	Period	Observation	Number of stations in TNB	Ave. Salinity ($\pm$ std) in a 10-m layer at 900-m depth
2014/15	11–16 Dec. 2014	Full-depth CTD/LADCP cast	11	34.796 ($\pm$ 0.001)
2015/16	8–15 Dec. 2015	Full-depth CTD/LADCP cast	10	34.791 ($\pm$ 0.007)
2016/17	26 Jan.–15 Feb. 2017	Full-depth CTD/LADCP cast	37	34.822 ($\pm$ 0.002)
2017/18	4–13 Mar. 2018	Full-depth CTD/LADCP cast	38	34.838 ($\pm$ 0.005)
DITN	**Period**	**Position**	**Depth [m]**	**Variables**
1st leg	12 Dec. 2014– 10 Dec. 2015	75° 21' 37" S, 164° 44' 58" E	75 (S, R) 275 (S, R) 660 (S, R)	S: 10 min T, C, P R: 30 min U, V
2nd leg	12 Dec. 2015– 08 Feb. 2017	75° 21' 36" S, 164° 44' 55" E	72 (S, R) 272 (S, R) 660 (S, R)	S: 10 min T, C, P R: 60 min U, V
3rd leg	09 Feb. 2017– 06 Mar. 2018	75° 21' 39" S, 164° 44' 47" E	74 (S, R, A) 272 (S, R, A) 665 (S, R, A)	S: 2 min T, C, P R: 60 min U, V A: 15 min T, P, U, V
DITD	**Period**	**Position**	**Depth [m]**	**Variables**
3rd leg	08 Feb. 2017– 06 Mar. 2018	75° 16' 33" S, 164° 04' 02" E	1208 (S) 1222 (A)	S: 2 min T, C, P A: 15 min T, P, U, V